European Journal of Chemistry

View Journal Online
View Article Online

Correlative analysis among experimental and theoretical structural, thermochemical, and molecular spectroscopic parameters of crystals of mandelic acid

Bojidarka Borisova Ivanova *

Lehrstuhl für Analytische Chemie, Institut für Umweltforschung, Fakultät für Chemie und Chemische Biologie, Universität Dortmund, Otto-Hahn-Straße 6, 44221 Dortmund, Deutschland

** Corresponding author at: Lehrstuhl für Analytische Chemie, Institut für Umweltforschung, Fakultät für Chemie und Chemische Biologie, Universität Dortmund, Otto-Hahn-Straße 6, 44221 Dortmund, Deutschland.*
e-mail: bojidarka.ivanova@yahoo.com (B.B. Ivanova).

RESEARCH ARTICLE

10.5155/eurjchem.17.1.1-12.2732

Received: 25 December 2025
Received in revised form: 1 January 2026
Accepted: 24 January 2026
Published online: 31 March 2026
Printed: 31 March 2026

KEYWORDS

Thermo chemistry
Mandelate crystals
Quantum chemistry
Bioorganic chemistry
Chemical crystallography
Density functional calculations

ABSTRACT

Crystals of mandelic acid are of significant importance. They are commercial pharmaceutical formulations that modulate the solubility of active ingredients and their pharmacological effect. Commercial medications have about 50% crystals. The salt formulation is among the most used strategies for improving the properties of therapeutics. Salt crystallization screening is implemented in the pharmaceutical industry. By disproportionation, free therapeutic forms are produced. The process is driven thermodynamically and kinetically. The method is addressed by crystallographic and quantum chemical methods for salt screening as integral parts of the development workflow in the pharmaceutical industry. Correlations among crystallographic, Fourier-transform infrared and electronic spectroscopic data on salts and theoretical thermo chemical approaches are of primary importance for determining the relations among the molecular structure properties of crystals. This paper presents novel structural and molecular spectroscopic data on mandelic acid such as DL-mandelic acid (1), 4-phenylpyridinium mandelate mandelic acid (2) and catena-((μ_3-DL-mandelato)-silver(I)) (3). It also utilizes chemometrics. The main conclusion follows from the relationship between the crystallographic potential energy data at the critical point of the bond using the Abramov formula and the theoretical bond dissociation energy showing |r|=0.9999. The approach seems to best describe the crystallographic energetics of the chemical bonds fitted off theoretical data.

Cite this: *Eur. J. Chem.* **2026**, *17(1)*, 1-12 **Journal website**: www.eurjchem.com

1. Introduction

Approximately a hundred years of ongoing pharmaceutical research documentation indicates that the programs for molecular drug design and screening of novel medications consist of a large number of development stages, including preclinical and clinical phases, crossing at about ten years. The commercial availability of new therapeutics also depends on its so-called dosage form. Determine the efficacy, side effects, or toxicity of therapeutics. The dosage form depends on many factors. The most important are the physicochemical properties of the drug in its pharmaceutical formulation. There are about 90% novel medications in the discovery pipelines of the pharmaceutical industry. Circa 40% of the marketed therapeutics suffers from low aqueous solubility [1-5]. Novel medication delivery approaches have been developed for oral solid dosage form of lipid-based pharmaceutics or injections. They are conventional and preferred in the patient delivery system, among others. The latter form is cost-efficient and is also easy to commercially manufacture. The pharmaceutical industry highlights the increase in the global market for oral solid dosage forms within 2017-2027 [6]. Thus, research effort focuses on the development of solid dosage forms of novel medications; thus, the barrier of drug solubility and its permeability issue. Until now, a set of research strategies have been developed that modulate the properties of medications in their solid forms. These are pH modification of analytes (co)-crystallizing as salts; co-crystallization of therapeutics and neutral species in crystals of pharmaceutical formulations; solid dispersions of components; polymeric micelles; inclusion complexes of embedded medication into biologically active macromolecules; solid lipid nanoparticles; particle size reduction and nanonization, micro emulsions, and more.

In particular, the concept of (co)crystallization of medications has been regulatory classified. Commercial pharmaceutical formulations of co-crystals are defined as crystalline materials containing two or more different molecules, one of which is medication within a defined stoichiometric ratio and crystal lattice. There are mutual nonionic and no covalent interactions. It is also determined the so-called polymorphism. It is a crystalline material of the same analytes, but exhibiting various packing. Crystal forms of medications that are most suitable for control of the physicochemical properties of the therapeutic drug and its

ISSN 2153-2249 (Print) / ISSN 2153-2257 (Online)
https://dx.doi.org/10.5155/eurjchem.17.1.1-12.2732

delivery. Thus, a significant amount in research efforts of crystal engineering are concentrated on the development of novel crystalline forms of therapeutics by modulating physico-chemical properties of analytes and improving their solubility, stability, permeability, bioavailability, and more; thus, achieving their improved therapeutic efficacy [2-5]. Innovations in crystal engineering involve strategies to pharmaceutical formulations *via* co-crystal or salt based on tuning of intermolecular interactions. An in-depth understanding of intermolecular interactions is essential in drug design and development. Achievement of desirable pharmacological properties of the active ingredient is imperative for pharmaceutical and clinical practice. Research practice involves various approaches to computing the properties of salt crystals. Data are validated by comparison with experimental data [7,8].

Herein lies the question: To what extent is an in-dept study of molecular conformation and spectroscopic properties of mandelic acid crystals (MA; (1)) (2-hydroxy-2-phenylacetic acid (1)? The issue has a significant impact on various fields of research on fundamental science and technology. It should only be sketched that MA is significant, due to: (I) its frequent use in pharmaceutical formulations [9,10]. It is a co-crystallizing agent or counter ion of salts of pharmaceutical formulations due to its low toxicity and cost, as well as readily availability on an industrial scale [11-13]. It is used in the commercial production of methenamine, which exhibits antibacterial prodrug biological activity against *Escherichia coli* [14]. The acidic properties of (1) (pK_{a1} = 3.4 [5]) promote urine acidification and; thus, promoting methenamine hydrolysis. (1) is also involved in pharmaceutical formulations of aripiprazole [5], trimethoprim [15], or baclofen [16]. The former medication is a third-generation antipsychotic drug [5]. Trimethoprim exhibits antimicrobial biological activity and is a synthetic agent that inhibits the bacterial dihydrofolate reductase enzyme [15]. The analyte treats muscle spasticity [16]. MA conformers have also been implemented in formulations with meloxicam, nicotinamide, meloxicam, levetiracetam or isoniazid, as well [15]. MA-based spirothiazolidinones are target agents against *M. tuberculosis* [17]. Co-crystallization of drugs with MA is governed by the fact that one of the important factors in obtaining an effective concentration of the active component; and, thus in producing a desirable pharmacological effect is solubility effect, [1,18]. Theoretical modeling of crystal growth of MA has been detailed in [7,8].

In addition, (*ii*) The chirality is a key issue in biological systems. A large number of biological processes are chirality-dependent ones. The biochemical reactions in living systems are highly enantioselective. Inappropriate molecular chirality might induce severe abnormalities. The pharmacological activity, metabolism, and toxicological effects of the enantiomers of drugs could differ drastically in humans [19]. Often, one enantiomer of therapeutics treats diseases, whereas its other enantiomer can induce a toxic or adverse side pharmacological effect. In the case of MA, enzymes of bacteria; for instance, *Pseudomonas species*, *Lactobacillus curvatus*, *Alcaligenes bronchisepticus*, and more show stereo-selective oxidation for MA and; thus, are used to chemically synthesize S-MA and R-MA enantiomers [20]. Stereo-selective metabolism of MA in the kidney and liver of rats shows that S-MA can be metabolized to phenyl glyoxylic acid as its main metabolite [20]. Therefore, chirality also has important implications in the pharmaceutical industry as well [21-23]. Utilizing enantiopure components into formulations is the most reliable approach to guarantee the effectiveness of medications. Although enantiomers show identical physicochemical properties, they exhibit different biological activities. Approximately 56% of market pharmaceuticals have a chiral center [24]. Approximately 94% of novel formulations that contain active ingredients containing the chiral center are enantiopure [24]. Thus, the cost-effective use of naturally occurring chiral molecules as components of pharmaceutical solids. The MA is also a promising template that allows for the design and synthesis of chiral co crystals and coordination polymers with metal ions *via* multiple binding centers and the capability of formation of chelate structures. So far, designed coordination polymers showing stereo-selective guest uptake and implementation in chiral separation technologies [21-23,25]. The MA chelating capability of metal ions is used to reduce calcium ion concentration *in vivo* as well.

The MA is also (iii) an attractive raw material used in the design of novel medications. There is an innovative class of MA-based medications that suppress the virulence of *Ralstonia solanacearum* [26,27], which is a soil-borne bacterium that causes a disease called 'bacterial wilt' and affects approximately 200 plant species, including commercial crops such as tomatoes, tobacco and potatoes. MA derivatives also suppress virulence by T3SS against Citrus canker [28], which is a highly contagious bacterial disease due to *Xanthomonas citri* subsp. To citrus crops. MA is an important chiral intermediate in the pharmaceutical industry for the synthesis of cephalosporins [20,29] and nafithromycin [30]. There are also novel MA-based peptidomimetics inhibiting aminopeptidase N, which is expressed in brain and kidney epithelial cells, among others [31].

As an α-hydroxy acid, (1) has also applications in (*iv*) dermatology due to its antibacterial properties [20,32-34]. MA also shows an antioxidant effect [25]. Lately, it has gained increasing popularity as a skin care treatment agent for adult acne [32].

The (*v*) enantioseparation of MA as α-hydroxy acids is also an essential process. Enantiomers are biomarkers for clinical diagnosis and prognosis of cancer, brain disease, and more [31]. MA is clinically determined to be a urinary metabolite of chronic kidney failure [35,36]. It is also used as a biomarker of styrene exposure, which is a dangerous environmental pollutant [20,37,38]. Vinyl MA is also routinely determined in thyroid cancer management [39].

In addition, (vi) MA importance should be emphasized for innovations in environmental cleaning technologies. Replacement of traditional petrochemical-based plastics [40,41] has led to an enormous search for green substitutes or so-called eco-friendly bioplastics. Poly(L-lactic acid), for instance, is a prospective biodegradable and biocompatible alternative as starch-based bioplastics [40,41]. However, these prospective biopolymers show poor crystallization kinetics; thus, limiting their applications. An improvement in crystallization capability is achieved *through* nucleating agents such as transition metal complexes of α-hydroxy acids such as mandelic acid [42]. As a natural [25] and environmentally friendly organic acid, MA shows high selectivity and efficiency in the reaction of hydrolysis of hemicellulose; thus making it a prospective candidate for the production of xylooligo-saccharides, as well [43,44].

Furthermore, a crucial advantage of MS is (*vii*) its capability of polymerizing; thus, it produces poly(mandelic acid), which itself is an aryl analogue of poly(lactic acid) and appears to be a biodegradable analogue of polystyrene. The synthetic scheme involves stabilization of MA-adducts with pyridine-containing bases for the mechanism of ring-opening polymerization reaction of MA. Its impressive advances show physical and mechanical properties of poly(mandelic acid) with polystyrene [45-48]. Thus, poly(mandelic acid) is also a potential bio-degradable plastic for hot-food packaging industry.

The interest in (*viii*) self-assembling processes of crystal MS, pyridine-containing counter ions, and transition metal ions has attracted further attention for the design of novel crystal topological networks of crystals [49]. Interest in MA crystals with pyridinium-containing ligands (ix) is governed not only by the MA capability of forming homopolymers, but also by the ability of pyridinium counter ions to produce [2+2] photo

dimerization products. The latter issue is an evergreen topic in crystal engineering of organics, due to their emergent photomechanical properties and a great scale of technological applications [50-52]. The key to experimental crystallographic knowledge of ionic interactions of MA and 4-phenylpyridine is the fact that the analyte appears to be an inhibitor of palmitoleoyl protein carboxylesterase [53]. I ts is an exogenous compound that can be found in oranges [54]. Owing to that it likely to across the blood brain barrier there is observed its methylation by nicotinamide N-methyl transferase. The accumulation of the latter analyte causes toxicity.

MA and its derivatives have also found place as modifiers for the asymmetric catalytic hydrogenation of ketopantolactone, for example [55] and for high-performance NiO_x-based perovskite solar cells [56]. So far, the application-oriented aspects of MA for many interdisciplinary research fields have been sketched, particularly highlighting the fields of pharmaceutical industry and medicine.

2. Experimental

2.1. Materials and methods

The single crystal X-ray diffraction intensities data on (1), (2) and (3) were measured on a Bruker Smart X2S diffractometer, utilizing micro-source Mo-Kα and ω-scan mode. An absorption correction approach was applied on multiple scanned reflections (Table 1). Structures were solved by direct methods using SHELXS-98 [57-63] and refined by the full-matrix least-squares refinement method against F^2. Anisotropic displacement parameters were used to non-hydrogen atoms. Hydrogen atoms joined with carbon atoms were placed at calculated positions. The refinement allows them to ride on the parent carbon atom. The H-atom connected with the oxygen one was manually constrained to positions. All H-atoms were placed at calculated positions with C-H distances of 0.95-0.99 Å, and treated as riding atoms with U_{iso}(H) = 1.1 U_{eq}(C). Their observation was confirmed from difference maps. The crystallographic structural data blocks were processed by PLATON [61]. The ADDSYM [61] test is used considering symmetry elements that scrutinize observable evidence regarding space group symmetry (Figures S1 and S2). It is a modified version of MISSYM software [64,65]. CheckCIF and PLATON are used to validate crystallographic reports [66,67]. The crystallographic refinement parameters are tabulated as shown above. The mono- and multipole electron density (ED) refinement was performed using the XD2016 and MoPro v16 program packages [68] employing the methodology developed by Hansen-Coppens. The experimental structural factors were also processed by WinGX 2014 [69] in relation to data quality. The WTANAL and DRK plot (Figure S3) analysis of the structure factors was carried out, in addition to the residual analyzes and THMA evaluation of thermal motion based on experimentally measured U_{ij} values [70,71]. The bond valence model and charge density analysis were performed by WinGX 2014 and Shelxle [72] program packages.

The infrared spectra of crystals within mid-region of electromagnetic spectrum (4000-400 cm^{-1}) were measured using a Bomem-Michelson 100 FTIR spectrometer (Bomem Inc., Canada) equipped with a Perkin Elmer wire-grid polarizer. Spectra were recorded with a resolution of ±0.5 cm^{-1} and 200 scans per spectrum. Nd:YAG laser was used (l_{max} = 1024 nm). The scan speed of the moving mirror was 0.5 $cm.s^{-1}$. Kbr-pellet and nujol mull techniques are utilized for sample preparation. Elemental analysis was carried out according to standard procedures for C and H (such as CO_2 and H_2O) and N (by the Dumas method). Scanning electron microscopy experiments were performed on a HITACHI S-3500N instrument.

Electronic spectra (UV-Vis-NIS) were recorded on Evolution 300 spectrophotometers, operating between 190 and 1100 nm in solution at a concentration of 3×10^{-6} M using 0.0921 cm quartz cells. Mass spectrometric measurements were performed with the TSQ 7000 instrument (Thermo Fisher Inc., Rockville, MD, USA). A triple quadruple mass spectrometer (TSQ 7000 Thermo Electron, 124 Dreieich, Germany) equipped with an ESI 2 source was used for ESI-MS and APCI-MS measurements (Table S1). A standard LTQ Orbitrap XL (Thermo Fisher Inc.) was employed. Absolute and relative intensities of the studied species were obtained using QualBrowser 2.7 software. Chromatographic analysis was performed with the Gynkotek HPLC instrument (Germering, Germany), equipped with a preparative Kromasil 100 C18 column (250×20 mm, 7 µm; Eka Chemicals, Bohus, Sweden) and a UV detector set at 250 nm. The experimentally measured raw crystallographic and spectroscopic data-files can be downloaded free of charge, herein [73].

2.2. Synthesis

The starting analytes 4-phenylpyridine and D,L-mandelic acid used to synthesis of 4-phenyl-pyridine (*bis*)mandelate (*bis*)mandelic acid (2) were Sigma-Aldrich products. Mixed equimolar amounts of the initial chemicals (0.155 and 0.152 g) were dissolved in 50 mL of CH_3OH. Thus, the solution obtained was stirred for 5 h at T = 100 ° C. The single crystals were filtered off, washed with CH_3OH and dried on P_2O_5 at T = 298 K. Yield 74%. Anal. Calcd for $C_{27}H_{25}NO_6$: C, 70.58; H, 5.48; N, 3.05%. Found: C, 70.55; and N, 3.01%. Single crystals of polymorph I of D,L-mandelic acid (1) were obtained after recrystallization of the powder analyte under ambient conditions in CH_3OH.

2.3. Theory/computations

GAUSSIAN 98, 09; Dalton2011 and Gamess-US [74-77] program packages were used. *Ab initio* and DFT molecular optimization were performed using the B3PW91 and B97X-D methods. The Truhlar's functional M06-2X was utilized. The algorithm by Bernys determines Gss. PES' stationary points were obtained *via* harmonic vibration analysis. Minima of energy are confirmed when there is a lack of the imaginary frequencies of the second derivative matrix. Basis set cc-pVDZ of Dunning, 6-31++G(2d,2p) and quasirelativistic effective core pseudo potentials from *Stuttgart-Dresden (Bonn) (SDD, SDDAll,* [http://www.cup.uni-muenchen.de/oc/zipse/los-alamos-national-laboratory-lanl-ecps.html] *were utilized.* The ZPE and vibration contributions have been accounted for up to a magnitude value of 0.3 eV. The species in solution were studied by explicit super molecule and mixed approach of micro hydration by PCM. The ionic strengths in solution were accounted for using IEF-PCM. Merz-Kollman atomic radii and heavy atoms UFF topological models were used. The pH effect was evaluated by computing properties in neutral and cationic forms. MD computations were performed by *ab initio* BOMD was carried out at M062X functional and SDD or cc-pvDZ basis sets, as well as, without to consider periodic boundary condition. The trajectories were integrated using a Hessian-based predictor-corrector approach with Hessian updating for each step on BO-PES. The step sizes were 0.3 and 0.25 $amu^{1/2}$Bohr. The trajectory analysis stops when: (a) Centres of mass of a dissociating fragment are different at 15 Bohr, or (b) when the number of steps exceeds the maximal number of points given as input parameter. The total energy was conserved during computations at least 0.1 kcal/mol. The computations were performed *via* fixed trajectory time speed (t = 0.025 fs) starting from initial velocities. The velocity Verlet and Bulirsch-Stoer integration approaches was used.

The Allinger's MM2 force field was utilized [78,79]. The low-order torsion terms are accounted for higher priority rather than van der Waals interactions.

Table 1. Experimental crystallographic refinement parameters on crystals.

Parameter	D,L-mandelic acid (polymorph I)	D,L-mandelic acid (polymorph I)	D,L-mandelic acid (polymorph II)	4-Phenyl-pyridine (*bis*)mandelate (*bis*)mandelic acid	Catena-((μ$_3$-DL-mandelato)-silver(I))
Compound	(1)			(2)	(3)
CCDC	880481	923825 (P=0.05 GPa)	923830 (P=0.76GPa)	822753	771414
Reference	[85]	[87]	[87]	This work	[119]
Formula	$C_8H_8O_3$	$C_8H_8O_3$	$C_8H_8O_3$	$C_{27}H_{25}NO_6$	$C_8H_6O_3Ag$
Mr	152.14	152.14	152.14	459.48	258.00
Crystal size	0.48×0.25×0.16	0.44×0.41×0.32	0.42×0.32×0.14	0.47×0.23×0.14	0.53×0.19×0.10
Crystal system	Orthorhombic	Orthorhombic	Monoclinic	Monoclinic	Monoclinic
Space group	Pbca	*Pbca*	$P2_1/c$	$P2_1/n$	$P2_1/c$
T [K]	198(2)	296(2)	296(2)	200(2)	300(2)
λ [Å]	0.71073	0.71073	0.71073	0.71073	0.71073
a [Å]	9.9537(15)	9.676(2)	5.825(2)	17.080(3)	16.274(3)
b [Å]	9.6632(15)	16.200(7)	28.908(11)	14.395(3)	4.7421(9)
c [Å]	16.173(3)	9.8866(19)	8.224(6)	19.408(4)	10.3421(19)
α [°]	90.00	90.00	90.00	90.00	90.00
β [°]	90.00	90.00	93.03(4)	96.648(7)	95.093(5)
γ [°]	90.00	90.00	90.00	90.00	90.00
V [Å]	1555.6(4)	1549.74	1382.9	4739.6(16)	795.0(2)
Z	8	8	8	8	4
μ[mm^{-1}]	0.100	0.100	0.113	0.091	2.492
r_{calc} [mg.m^{-3}]	1.299	1.304	1.462	1.288	2.156
2θ [°]	25.10	28.36	27.67	25.07	25.03
Refl. collect.	8941	5614	4768	5830	1401
Unique refl.	1386	535	684	614	1107
Obs. refl. [I>2σ(I)]	1386	386	598	614	1401
GOF on F^2	0.796	1.297	1.335	1.359	0.860
R_1 [I > 2σ(I)]	0.0410	0.1421	0.2052	0.0632	0.0408
wR_2 (all data)	0.0580	0.2142	0.2242	0.1029	0.0670
Residuals [e.Å^{-3}]	0.119/-0.171	0.110/-0.142	0.281/-0.265	0.446/-0.282	0.696/-1.417

The method's accuracy is 1.5 kJ/mol of diamante or 5.71.10^{-4} a.u. The electronic spectra were calculated using equation-of-motion coupled cluster with single and double substitutions approach. It is regarded as the gold standard tool for reliable excited state computations [80-82]. The effect of the ionic strength is also accounted for [83].

2.4. Chemometrics

Statistical methods or chemometrics were applied to experimental and theoretical data. It was done by R4Cal OpenOffice STATISTICs for Windows 7 program packages [84]. The statistical significance of each regression coefficient was verified by the *t*-test. The adequacy of the model was determined by *F*-test for goodness of fit and lack-of-fit, respectively. The analysis of variance method was also used. The non-linear fitting of the experimental MS data was carried out using the search method based on the Levenberg-Marquardt algorithm.

3. Results and Discussion

3.1. Molecular and crystal structural data

Polymorph I of DL-mandelic acid (1) crystallizes into orthorhombic space group type *Pbca* under ambient experimental conditions [85-93] (Figures 1, S4, and S5; Table 1). Its high pressure polymorph II shows monoclinic space group type $P2_1/c$ [86,91]. The intermolecular interactions lead to hydrogen-bonded double chains of MA-molecules along the a-axis. Its crystal structure is markedly different from polymorph I [91]. The polymorphism accounts for the molecular capability to crystallize in more than one crystal structure depending on the packing properties of molecules due to their intermolecular interactions [94-98]. The properties of polymorphs could vary with respect to molar volume; crystal density; refractive index; hygroscopicity; and more. They are associated with thermodynamics; kinetics; surface and mechanical properties of crystals. The phenomenon becomes an important task for the manufacture of pharmaceuticals [86,87,99]. There is a polymorph transition of MA at P = 0.65 Gpa and at T = 460 K. This study lacks a description of intramolecular interactions of (1) in crystals.

For the reasons sketched above, this study discusses novel data on experimental and theoretical ED analyzes and electrostatic surface potential (ESP); thus, aiming at in-depth understanding of the relation among molecular and electronic structures↔crystal structue↔properties of (1). The latter relations determine both the biological and catalytic activity. In particular, MA-derivatives show unusually complex packing in crystals. Furthermore, there is a small energy difference between polymorphs [100]. It also determines a significant structural and bulk and surface diversity, as well. The same is valid to disorder MA showing a drastic variety of disordered structures and their energetics. Computations accounting for environmental effects; for instance, temperature, ionic strength, and more, are of primary importance by considering application-oriented aspects. Because of, they affect on energetics of various hydrogen bonded MA structural motifs. The focus of the studies underlines the relationship between molecular and crystal structure as well as spectroscopic properties. Thus, the relationships between crystallographic and theoretical data on electronic structures or the ED distribution of atoms in molecules among MA- crystals should be considered. Electronic interactions determine electronic absorption spectra and vibration characteristics of molecules within the concept of chemical bond [101].

The distribution of Eds is important for understanding the mechanisms of chemical reactions and, respectively, the biological activity of species. The thermodynamic approach assesses the energetics of electronic interactions of species *via* enthalpy reflecting the energetics of chemical bonds and entropy accounting for environmental factors. There is a direct relationship between molecular structure (hydrogen) bonding interactions↔energetics with measured IC_{50} or the so-called transfer function [102-104]. Thus, experimental and theoretical electronic structural analysis of interatomic and, respectively, intermolecular interactions in molecules and their crystals reveal the actual dimension of the study ranging from the determination of experimental ED of atoms in molecules to their biological function only by assessing the aforementioned correlation quantitatively.

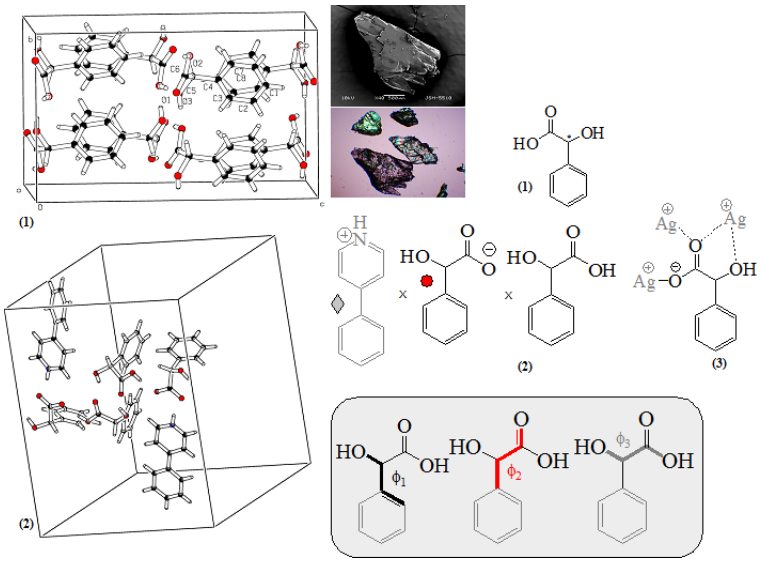

Figure 1. ORTEP plots of the unit cell contents of crystals (1) (CCDC 880481) [85] and (2) (CCDC 822753) (this work); chemical diagrams of crystals (1)–(3); name definitions of the dihedral angles of mandelic acid; photograph and scanning electron microscopic image of crystals.

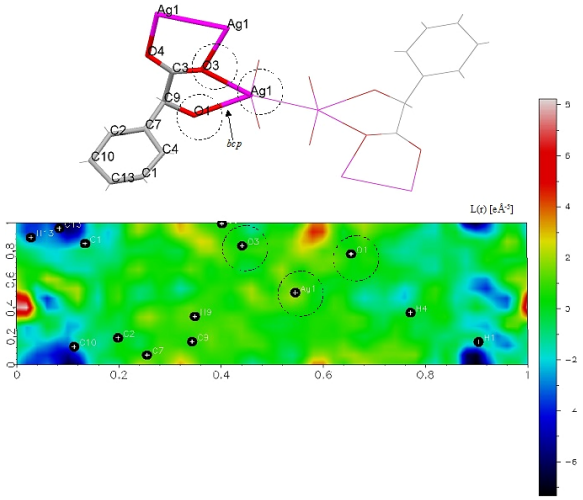

Figure 2. 2D map of Laplacian of electron density L(**r**) [electron.Å^{-5}] of (3); molecular crystallographic structure of (3) and atom labelling scheme.

The crystallographic ED distribution looks at the electronic charge distribution around atoms in molecules [101]. The distribution of total molecular charge distribution in crystal is determined using atomic positions within the 3D space, their thermal vibrations, and electronic charge parameters [105-108]. The models are fitted by means of least squares of crystallographic data. The mapped electrostatic properties in both the 2D and 3D space (Figures 2 and Figure S4) can be obtained *by* crystallography and computational tools. There is a link between experimental and theoretical 3D electronic structures. Important parameters, among others, are electrostatic potentials (ESPs). They are derived from crystallographic data or computational methods. The ESP maps (Figure 3) illustrate regions of electro negativity and positivity. The regions are not easily inferred from the analysis of the parent charge density distribution. The ESP map on *Hirshfeld surfaces* details on intermolecular interactions of crystals [109-114]. They define the 3D space occupied by molecules; thus, partitioning the ED crystal into molecular fragments of crystals.

Bader's quantum theory of atoms in molecules used to obtain experimental EDs [115]. Although the theories provide crucial knowledge of the molecular structure of crystals, thus attracting the explanation and prediction of intermolecular interactions, their direct application is far from trivial. It might not be so intelligible to apply them directly. If there is a concentrate on Hirshfeld surfaces, then the weight function of crystal molecules depends on diffusion properties of the atoms [115]. Therefore, an accurate prediction of Hirshfeld atomic charges *via* depends on the theoretical level.

However, precise determining of the experimental and theoretical Eds plays a crucial role in describing the nature of chemical bonds of molecules or their energetics, and thus the properties of molecules and crystals. Because Hirshfeld surface analysis (HAS) is broadly utilized for quantifying intermolecular interactions of molecules in crystals, it appears clear to us that, depending on the accuracy of the data, the analysis could be plausible or could not. There should be looked for further criteria for reliable description of interatomic and intermolecular interactions of crystals to determine plausibly their energetics and properties.

Thus, first this study correlates among crystallographic thermal parameters of MA in crystals (1) and (2) (Table S1) Figure S6 correlates coefficients S and h.

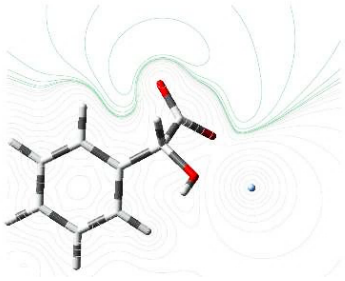

Figure 3. Theoretical (M062X/LANL2DZ) electrostatic potential 2D map of (3).

The former parameter denotes the (isotropic) variance of the mean square amplitude U, while h is defined by Hirshfeld and Shmueli [116]. There are obtained |r|=0.98 and 0.892. The reliability of measurands depends on quality of crystallographic data-block of variables. It could vary from measurement to measurement. The relative contribution to parameters such as random and systematic errors; intramolecular vibrations, and more have been detailed in work [116].

The crystallographic thermal parameters of each atom describe fluctuations of the ED around average atomic positions. The fluctuations are random and cannot be theoretically predicted. The crystallographic data provide a statistically averaged molecular structure which fluctuates in time and 3D space. Thus, the study involves both static and molecular dynamics (MD) computations of the crystals (Figure S7). Depending on the complexity of the molecules, an anharmonic contribution could be added. Anharmonicity contributes to systematic error of the molecular model, as well [117]. The molecular vibration of crystals is a temperature-dependent process. The functional relation was established by Cruickshank (1956) [118]. Depending on the temperature of crystallographic measurements, there is further variation of the collected data block of experimental variables of molecules in crystals.

Mostly, molecular structures of crystals of an analyte are equated with the absence of uncertainty parameters. However, they have an effect on both the experimental and theoretical interactions, parameters, and properties. The atomic positions reflect maximum of X-ray scattered density. It is fitted to the ED distribution. Thus, crystal structures could be equated only in cases of negligible thermal displacement parameters. As Figure S6 reveals, variation can be from crystal structure to crystal structure even by studying the same MA dimers of crystals (1) and (2), due to the symmetry operation (−*x*+2, −*y*+1, −*z*) generates the whole system of (2). It crystallizes in space group type $P2_1/n$ showing unit cell parameters *a*=17.080(3), *b* = 14.395(3), *c* = 19.408(4) Å, *β* = 96.648(7)°, *Z* = 12, *V* = 4739.6(16)Å^3. The crystal structure of (2) was solved by direct methods and refined by full-matrix least-squares on F^2 to final values of R_1=0.0667 and wR_2=0.1046. In (2), species are linked to the 3D network through moderate N^+-H···O hydrogen bonds r(N···O)= 2.741, 2.717 Å (Figures 1, and S7; Table 1). Anions and neutral MA form stable self-associates *via* moderate OH···O bonds r(O···O)=2.494, 2.535 Å. Two neutral MA molecules in (2) form a dimer through OH···O bond r(O···O) = 2.837 and 2.879 Å. The cations exhibit two different molecular conformations that show interplanar angles of the phenyl and pyridinium fragments −27.08° and 1.30° (Figures S8 and S9). The MA conformations in crystals (1)–(3) are shown in Table S2.

Despite theoretical models connecting among simulated ensembles of molecules and crystallographic data, frequently, they cannot count precise crystallographic parameters, due to variation within replicates; if any. The failure is grounded to various factors and error contributions. In order to obtain convergence of view, how reliably to draw line between models and crystallographic experiment there is applied theoretical tools; thus, assessing best description of experimentally phenomena *via* chemometrics.

Therefore, experimental and theoretical ED and energetics of Ag^I-complex of MA (3) are discussed as well. Its crystallographic parameters could be found [119] together with electronic spectra [85]. Briefly, the Ag^I-ion of the dinuclear Ag^I-containing substructure is connected to four O atoms, having an Ag–O bond distance r(Ag···O)=2.215–2.492 Å (Figure S10). The inter-ionic Ag^I–Ag^I interaction shows that *r*(Ag···Ag)=2.820 Å. The MA anion acts as a tridentate ligand *via* deprotonated COO- and OH-groups. The COO^- ion is bonded to two Ag^I-ions in a dinuclear subunit. The OH group appears to be bridged by the ligand center, coordinating each of the binuclear cores; thus, forming a coordination polymer. The Ag^IO_5 metal chromophore has a distorted trigonal pyramidal structure. This study specifies measured crystallographic variables and their complementary treatment with quantum chemistry data; thus, it is discussed novel data on energetics from crystallography. This line of research is particularly strengthened if experimental and theoretical ED of atoms in the molecule of (3). The real ED values of the atoms in molecules within 3D space are determined using the least squares refinement ED parameter ED r(r) [120]. The F_o-maps reflect experimental ED at each point of the 3D space. In addition to the 2D ED distribution, there is a 3D ED one.

There are evaluated rho(r) (or r(r)) and Laplacian_rho(r) (or L(r)) of experimental ED of atoms (Figure 2). The ESP surface of (3) and the M062X/LANL2DZ level of theory is depicted in Figure 4. Knowledge of the nature of interatomic interactions in molecules or the metal-to-ligand coordination of the Ag^I ion with O-center from MS by crystallography imports reliable statistical assessment of r(r) and L(r) values between interacting species. Therefore, when there are predominat ionic M–L interactions, then the rho(r) values are within the 0.2–0.3 eÅ^{-3} [121]. In the cases when rho(r) > 0.6 e Å^{-3} there is a predominantly covalent M–L bond. Owing to the fact that there is statistical assessment of uncertainty of experimental crystallographic datasets of variables, the reliability of absolute quantification of experimental ED of atoms or rho(r) data on depends on reliability of Laplacian_rho (r). It is determined using experimental crystallographic factors reflecting the completeness of Fourier series and amplitudes quality; and, model of ED distribution [122].

Therefore, reliability of rho(r) and Laplacian_rho(r) is connected with the quality of *hkl* reflections and refinement model. The quality of data-blocks of measurands depends on the resolution of measurements; single crystal and its scattering properties. There are also permanent random errors of measurements as a result of fluctuation of atomic vibration factors. Thus, our knowledge of nature of intermolecular interactions, including metal-to-ligand ones obtained *via* crystallography, is a correct one. It is not absolute knowledge.

Table 2. Critical point analysis of bonds of the crystals of compound 3; Laplacian electron density L(**r**) [electron.Å^{-5}]; electron density r(**r**) [electron. Å^{-3}]; l_1 – parameters (I = 1–3) (L(**r**) = l_1 + l_2 + l_3); intermolecular saddle (3,-1) critical points are described; the interactions with H-atoms are omitted; atom labelling scheme (Figure 2).

Atom 1	Atom 2	r(r)	L(r)	l_i, i = 1–3			Ellipticity (e)
				l_1	l_2	l_3	
Ag1	O1	0.2411	4.00	-0.92	-0.90	5.82	0.0170
Ag1	O3	0.2068	3.34	-0.74	-0.74	4.81	0.0067
O1	C9	1.4501	4.42	-7.60	-7.59	19.61	0.0012
O3	C3	1.8884	-3.23	-9.74	-9.59	16.09	0.0154
O4	C3	2.0915	3.83	-11.08	-10.91	25.82	0.0154
C1	C4	1.4311	-1.35	-6.71	-6.44	11.80	0.0412
C1	C13	1.7817	-7.35	-8.55	-8.27	9.47	0.0346
C2	C7	1.4228	-1.34	-6.67	-6.41	11.74	0.0402
C2	C10	1.5170	-2.72	-7.18	-6.93	11.40	0.0359
C3	C9	1.2828	0.39	-5.79	-5.78	11.95	0.0024
C4	C7	1.4939	-2.39	-7.05	-6.80	11.47	0.0368
C7	C9	1.3293	-0.10	-6.07	-5.95	11.92	0.0198
C10	C13	1.3169	0.07	-6.09	-5.83	11.99	0.0448

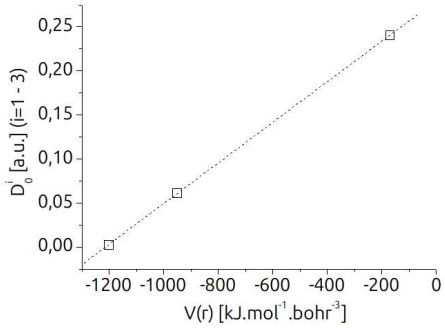

Parameter	Value	Error	
A	0.28016	7.76904.10^{-4}	
B	2.30783.10^{-4}	8.7238.10^{-7}	
|r|	sd(yEr±)	N	*p*
0.99999	6.64014.10^{-4}	3	0.00241

Figure 4. Correlation between theoretical DFT and experimental data on crystals; chemometrics.

The rho(r) is a probability function of experimental ED. It is not an absolute quantity of ED at the point (x, y, z) of the 3D space. Therefore, a precise study of the nature of neither M–L bonds nor intermolecular hydrogen bonding or short contacts cannot be achieved even by processing high-quality crystallographic data-blocks of variables. The theory also implies that Laplacian_rho(r) (and gradient_rho(r)) reflects the so-called *bond paths* or boundaries of interacting species [123-131]. The charge-density models allow for the evaluation of realistic interatomic, respectively, intermolecular interactions of crystals. The interacting species are described as chemically bound when there are different (3, -1) so-called *bond critical points* (bcp) in rho(r) between them [130]. When Laplacian_rho(r) values < 0, there is charge concentration. A Laplacian_rho(r) > 0 means charge depletion. The Laplacian_rho(r) is given by the sum of the l_i parameters. The parameter ellipticity (e) details the bond order of the interactions. When there is s-bond, then l_1–l_2 cause for bcp=0 because l_1 and l_2 are mutually perpendicular to chemical bond axes within the cylindrical symmetry approximation along the bond axis. The increase in bond order causes an increase in ellipticity. The results from crystal (3) (Table 2) show e=0.0170 and 0.0067 of Ag^{I}-O^{1} and Ag^{I}-O^{3} interactions. The values are relatively large compared to purely ionic interactions. There is assumed a charge delocalization. The latter experimental data are correlated with theoretical natural ionicity parameter (i_{AB}) determined according to Equation S1 [125]. It is calculated using M062X/LANL2DZ natural polarization coefficients (c_A, c_B) obtained from (3) and summarized in Table S3. There is $i_{Ag\text{-}O1}$=-0.0544, which confirms crystallographic results and indicates a charge delocalization effect. The value is higher compared to $i_{Zn\text{–}Cl}$ one of -0.76 determined from the [$(ZnCl_4)^{2-}$] counter ion containing crystals of coordination compounds [132]. The species show almost purely ionic Zn–Cl bond and ionic hybrid localized at the Cl-center. The C–O bonds of MA of (3) show $i_{C\text{–}O}$ = 0.4386–0.1853.

Furthermore, detail on the nature of interatomic and intermolecular interactions of crystal species has been associated between interaction energy and rho(r) at bcp. It is approximated linearly [119,132]; thus, stressing the important correlation between the characteristic of the the M-L bond and the energy of interaction. Among the models that connect crystallographic ED, expressed by Laplacian and energy, there is the Abramov's model Equation (1) [131,133]. The G(r) denotes the electronic kinetic energy. The V(r) value means the potential energy at *bcp*. It is used to study the complex (3) (Table 3) because within a series of Ag^{I}-, Cu^{II}-, and Zn^{II}-complexes of organics it has been found that V(r) depends linearly on the theoretical dissociation energy D^{i}_{0} of the i^{th} chemical bond of crystal molecules [119,132,134].

$$¼(L(\mathbf{r}))=2G(r)+V(r) \quad (1)$$

This study also treats the relationship V(r) = *f*(D^{i}_{0}) of the Ag^{I}-complex of MA (3). The correlation between the experimental bond energy parameters of equation (1) of V(r) (Table 3) and the theoretical parameters D^{i}_{0} (Figures S11 and S12) as well as the M062X / LAL2DZ energetics of species (Table S4) yields excellent performances, showing |r| = 0.9999 (Figure 4) Theoretical bond dissociation energy and the potential energy of bonds in bcps allow for reliable correlation among theoretical and experimental properties and energetics of the molecules in crystals.

Table 3. Topological energetics of the complex 3 using experimental electron densities; G_{cp} – Kinetic energy at bcp [a.u.Bohr^{-3}]; V_{cp} – Potential energy at bcp [a.u./bohr^{-3}] or [kJ.mol^{-1}.bohr^{-3}]; intermolecular saddle (3,-1) critical points are described; the interactions with H-atoms are omitted; atom labelling scheme (Figure 2).

Atom_1	Atom_2	G_{cp} [a.u.Bohr^{-3}]	V_{cp} [a.u.Bohr^{-3}]	G_{cp} [kJ.mol^{-1}.Bohr^{-3}]	V_{cp} [kJ.mol^{-1}.Bohr^{-3}]
Ag1	O1	0.03878	-0.03608	101.82	-94.73
Ag1	O3	0.03170	-0.02878	83.22	-75.55
O1	C9	0.25190	-0.45797	661.35	-1202.40
O3	C3	0.32141	-0.67633	843.87	-1775.71
O4	C3	0.43401	-0.82829	1139.49	-2174.68
C1	C4	0.20722	-0.42842	544.05	-1124.81
C1	C13	0.26115	-0.59855	685.65	-1571.50
C2	C7	0.20519	-0.42428	538.72	-1113.94
C2	C10	0.21980	-0.46783	577.08	-1228.30
C3	C9	0.18313	-0.36224	480.80	-951.06
C4	C7	0.21610	-0.45694	567.36	-1199.69
C7	C9	0.19078	-0.38259	500.90	-1004.48
C10	C13	0.18903	-0.37729	496.30	-990.57

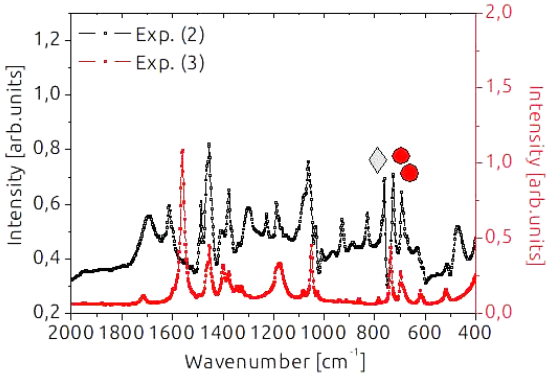

Figure 5. Experimental solid-state IR spectra of complexes 2 and 3.

Because the experimental and theoretical design, herein, is governed by the so-called means-end-reasoning, further, it concentrates on Hirshfeld atomic charges and populations. They are essential for modeling of the physicochemical properties of molecules (Tables S5 and S6). There are also used ESPs. The correlation between Hirshfeld atomic charges and populations of (3) shows |r|=0.7007.

Since a particular focus on this study is on accurate tools for theoretical and experimental description and prediction of atomic, respectively, molecular interactions of crystals, it should be highlighted that the Hirshfeld population analysis can be used for exact determination of molecular dipole moments and higher multipole ones.

One needs a simple representation of charge redistribution of molecules using only atomic charges, the so-called monopole approximation. This is the case, for instance, when Hirshfeld charges are mapped on a novel set of charges reliably representing the ESPs, but without taking into account atomic dipoles, because ESPs accurately predict the chemical reactivity of species [114]. This study also uses the Truhlar's charge models called CM5 [135]. The correlation between Hirshfeld and CM5 charges shows |r|=0.98531.

The analysis between Hirshfeld charges or CM5 charges and ESP of (3) yields |r|=0.1791. The low performances are due to the deviation of the ESP value of the Ag^{I}-ion. There is |r|=0.99561 of the same data when the ESP value of the metal ion is excluded. The latter rather controversial data are explained by the fact that in (3) there is charge delocalization, as both crystallographic and theoretical natural bond orbital analysis data have shown, above.

Therefore, the metal-to-ligand charge delocalization effect of Ag^{I}-complexes should be tackled by using complementary both ESP and atomic charges, respectively, electron densities. Natural polarization coefficients should be accounted for; thus, allowing for an in-dept characterization of the nature and energetics of the coordinative metal-to-ligand bond.

3.2. Optical spectroscopic data

Vibration spectroscopy [136-138] is a robust tool for structural analysis of solids, including crystals in pharmaceutical industry Figures 5, S13-S15 depict experimental solid state and theoretical (M062X/LANL2DZ) IR-spectra of crystals (2) and (3). The vibration modes of the racemate and enantiopure forms of (2) have been detailed in [136]. The IR spectrum of (1) is detailed in [85].

The IR spectrum of (2) exhibits a ν_{OH} stretching vibration at 3460 cm^{-1} of MA. The $\nu_{C=O}$ mode is at 1695 cm^{-1}. The low-frequency shifting of mode comparing with data on (1) and those ones reported previously [136] at 1714 cm^{-1} is result from shorter C–O bond of acid in crystals of (2) exhibiting bond length *r*(C–O)=1.236–1.259 Å while data on (1) is *r*(C=O)=1.207 Å.

There is a deprotonated COOH-group of MA in the former crystal. There are asymmetric intermolecular interactions causing or distorting local C_{2v} symmetry of the carboxylate anionic structural subunit. The intensive IR band at 693.069±0.53 cm^{-1} belongs to the out-of-plane bending vibration of the monosubstituted phenyl fragment of MA. There is a difference in Δν=|2| cm^{-1} compared with the MA racemate results. There is agreement with data on work [136] showing a value of 695 cm^{-1}. The bands at 764.64±0.3 and 727.64±0.25 cm^{-1} belong to 4-phenylpyridinium counter ion.

IR spectroscopy is implemented in the pharmaceutical industry as a reliable tool for the structural analysis of multicomponent formulations, including MA-ones [137]. The IR pattern is complicated (Figure 5) As the curve-fitted spectrum of (2) reveals, there are $\nu_{C=O}$ and $\nu^{as}{}_{COO^-}$ modes within the 1800-1500 cm^{-1} region due to the presence of both neutral MA and its anion. An in-depth vibration analysis of the co-crystals and salts of MA *via* IR spectroscopy [137] has assigned IR-band at 1732 cm^{-1} to the νC=O mode of the S-MA enantiomer, while the band at 1704 cm^{-1} to νC = O of R-MA form. The band at 1669 cm^{-1}

belongs to ν_{COO^-} mode. However, the IR-spectra of crystals of (2) and (3) containing MA anion herein show IR-band at 1616 cm^{-1} in (2) assigned to $\nu^{as}_{COO^-}$ stretching mode. It is shifted to 1561 cm^{-1} in (3) due to coordination of the MA-anion with the Ag^{I}-ion. The shifting of $\Delta|\nu|=55$ cm^{-1} further supports the ED data and the natural ionicity parameters showing that the Ag–O bond of (3) is characterized with significant charge de-localization; thus, there is a lack of purely ionic interactions of the MA-COO- and Ag^{+} species. The phenomenon is observed in Zn^{2+} complexes with chalcogenide ligands [132].

Figure 6 shows theoretical and experimental EOM-CCSD data on MA and crystals (1)-(3) (Table S7) The charge transfer effect is evaluated *via* long-range transition densities, as well. There is difference in the theoretical and experimental absorption maxima $\Delta|\lambda_{max}|$ = 10 nm. The experimental data on MA agree well with the previous study of MA in aqueous solution showing λ_{max}=218 nm, assigned to the $n \rightarrow p^*$ transition [139]. The experimental data on crystal (2) show λ_{max}=269 and 290 nm. This indicates that the bands belong to the $n \rightarrow p^*$ and $p \rightarrow p^*$ transitions of the protomer. The band at λ_{max}=225 nm of (3) is assigned to charge transfer one due to coordination of MA with Ag^{I}-ion.

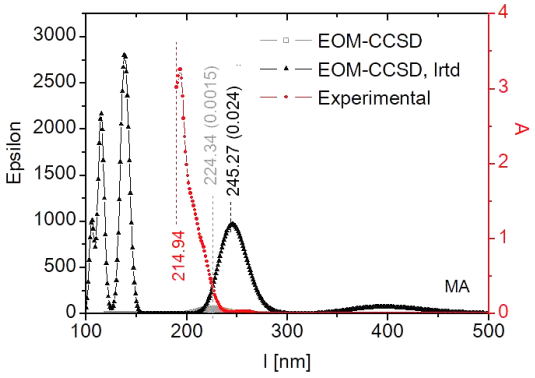

Figure 6. Theoretical EOM-CCSD spectra of mandelic acid together with its experimental electronic absorption spectrum in CH_3OH.

However, complex (3) is unstable in solution. Its mass spectrometric analysis has been detailed in [140]. The Ag^{I} ion preferably forms solvate complexes. MS peaks were observed at *m/z* 278.04 and 280.04 of the $^{107/109}Ag$ complex of MA (Figure S16). The highlight is that there could be failure in assigning experimental spectra of crystals in solution because of the correlation of electronic absorption properties of various processes, particularly, looking at coordination compounds where competitive ligand exchange of solvent molecules is frequently occurring.

4. Conclusions

(A) First, this study reports crystal structure of 4-phenylpyridinium mandelate mandelic acid (2). It is completely characterized by means of single crystal X-ray diffraction, electronic absorption, and vibration spectroscopy both experimentally and theoretically.

(B) The data on point (A) of the crystals of salts of mandelic acid have been correlated with the novel experimental and theoretical electron density analysis of crystals of the Ag^{I} complex of mandelic acid; thus, assessing the relationship between crystallographic potential energy data on the critical point of the bond according to the Abramov model and the theoretical dissociation energy of the bond. The best method performance shows |r|=0.9999. The tool seems to best characterize experimental crystallographic energetics of chemical bonds of molecules fitted off high-accuracy methods of quantum chemistry.

Acknowledgements

The author is grateful to the Deutscher Akademischer Austauschdienst (DAAD) for the donation of the Evolution 300 UV–Vis–NIR spectrometer; the Alexander von Humboldt Foundation for the grant and the donation of a single-crystal X-ray diffractometer to the "Molecular Spectroscopy and Structural Analysis" Laboratory, Department of Analytical Chemistry, Sofia University "St. Kl. Ohridski"; the Deutsche Forschungsgemeinschaft (Grant No. 255/22-1); and the Central Instrumental Laboratory Cluster for Mass Spectrometry at the Institute of Environmental Research, TU Dortmund University.

Supporting information

CCDC 822753 (2) contains supplementary crystallographic data for the crystal. The crystallographic information files can be obtained free of charge *via* http://www.ccdc.cam.ac.uk/conts/retrieving.html or from Cambridge Crystallographic Data Centre, 12 Union Road, Cambridge CB2 1EZ, UK; fax: (+44) 1223-336-033; or e-mail: deposit@ccdc.cam.ac.uk Supplementary data associated with this paper can be found, in the online version.

Disclosure statement

Conflict of interest: The authors declare that they have no conflict of interest.
Ethical approval: All ethical guidelines have been adhered to.
Sample availability: Samples of the compounds are available from the author.

ORCID and Email

Bojidarka Borisova Ivanova
bojidarka.ivanova@yahoo.com
https://orcid.org/0000-0002-5788-4404

References

[1]. Euldji, I.; Si-Moussa, C.; Hamadache, M.; Benkortbi, O. QSPR Modelling of the Solubility of Drug and Drug-like Compounds in Supercritical Carbon Dioxide. *Mol. Inform.* **2022**, *41* (10), 2200026 https://doi.org/10.1002/minf.202200026.
[2]. Kumari, N.; Ghosh, A. Cocrystallization: Cutting Edge Tool for Physicochemical Modulation of Active Pharmaceutical Ingredients. *CPD.* **2020**, *26* (38), 4858–4882.
[3]. Duggirala, N. K.; Perry, M. L.; Almarsson, O.; Zaworotko, M. J. Pharmaceutical cocrystals: along the path to improved medicines. *Chem. Commun.* **2016**, *52* (4), 640–655.
[4]. Almarsson, O.; Zaworotko, M. J. Crystal engineering of the composition of pharmaceutical phases. Do pharmaceutical co-crystals represent a new path to improved medicines?. *Chem. Commun.* **2004**, *17*, 1889–1896.
[5]. Shah, H. S.; Michelle, C.; Xie, T.; Chaturvedi, K.; Kuang, S.; Abramov, Y. A. Computational and Experimental Screening Approaches to Aripiprazole Salt Crystallization. *Pharm Res* **2023**, *40* (12), 2779–2789.
[6]. Gupta, D.; Bhatia, D.; Dave, V.; Sutariya, V.; Varghese Gupta, S. Salts of therapeutic agents: Chemical, physicochemical, and biological considerations. *Molecules* **2018**, *23*, 1719.
[7]. Tan, Q.; Hosseini, S. A.; Thévenin, D. Simulations of crystal growth using lattice Boltzmann formulation. In *High Performance Computing in Science and Engineering* '22; Springer Nature Switzerland: Cham, 2024; pp. 387–398.
[8]. Tan, Q.; Hosseini, S.; Seidel-Morgenstern, A.; Thévenin, D.; Lorenz, H. Thermal effects connected to crystallization dynamics: A lattice Boltzmann study. *Int. J. Multiph. Flow* **2024**, *171*, 104669.
[9]. Nechipadappu, S. K.; Swain, D. New drug–drug and drug–nutraceutical salts of anti-emetic drug domperidone: structural and physicochemical aspects of new salts. *CrystEngComm* **2024**, *26* (7), 926–942.
[10]. Zhou, J.; Wei, Y.; Wu, J.; Li, S.; Xu, Z.; Peng, Y. Novel ethylenediamine-β-cyclodextrin grafted membranes for the chiral separation of mandelic acid and its derivatives. *Chirality* **2024**, *36* (4), e23662. https://doi.org/10.1002/chir.23662.
[11]. Tenorio, J. C.; Alves, D. C.; Carvalho Jr, P. S. Diastereoisomeric double salts of Carvedilol with (L)- and (D)-mandelic acids. *J. Mol. Struct.* **2025**, *1325*, 140909.
[12]. de Meester, J.; Layrisse, P.; Marchivie, M.; Collard, L.; Wery, G.; Brandel, C.; Cartigny, Y.; Subra-Paternault, P.; Leyssens, T.; Harscoat-Schiavo, C. Towards a new approach in chiral resolution: Pressurized-CO2 assisted preferential cocrystallization. *J. Supercrit. Fluids* **2024**, *212*, 106339.

[13]. Martínková, L.; Křen, V. Biocatalytic production of mandelic acid and analogues: a review and comparison with chemical processes. *Appl Microbiol Biotechnol* **2018**, *102* (9), 3893–3900.

[14]. Li, J. M.; Cosler, L. E.; Harausz, E. P.; Myers, C. E.; Kufel, W. D. Methenamine for urinary tract infection prophylaxis: A systematic review. *Pharmacotherapy* **2023**, *44* (2), 197–206.

[15]. Fitriani, L.; Arif, Z.; Hasanah, U.; Zaini, E. Enhancing the Solubility and Dissolution Rate of Tenoxicam through Co-Amorphous Formation with Meglumine by a Solvent Dropped Grinding Method. *Sci. Technol. Indones.* **2025**, *10* (1), 131–138.

[16]. Songsermsawad, S.; Nalaoh, P.; Promarak, V.; Flood, A. E. Chiral Resolution of*RS*-Baclofen via a Novel Chiral Cocrystal of*R*-Baclofen and*L*-Mandelic Acid. *Cryst. Growth Amp; Des.* **2022**, *22* (4), 2441–2451.

[17]. Trawally, M.; Demir-Yazıcı, K.; Dingiş-Birgül, S.; Kaya, K.; Akdemir, A.; Güzel-Akdemir, O. Mandelic acid-based spirothiazolidinones targeting M. tuberculosis: Synthesis, in vitro and in silico investigations. *Bioorg. Chem.* **2022**, *121*, 105688.

[18]. Vimalson, D. C. Techniques to enhance solubility of hydrophobic drugs: An overview. *Asian J. Pharm.* **2016**, *10*, S67-75. https://www.asiapharmaceutics.info/index.php/ajp/article/view/625

[19]. Chen, W.; Qiu, X.; Chen, Y.; Ke, J.; Ji, Y.; Chen, J. Supramolecular Interaction Modulation in Thermosensitive Composites: Enantiomeric Recognition and Chiral Site Regeneration. *Anal. Chem.* **2024**, *96* (14), 5580–5588.

[20]. Zhang, Y.; Su, C.; Lei, J.; Chen, L.; Hu, H.; Zeng, S.; Yu, L. Studies on the L-2-hydroxy-acid oxidase 2 catalyzed metabolism of S-mandelic acid and its analogues. *Drug Metab. Pharmacokinet.* **2019**, *34* (3), 187–193.

[21]. Tay, H. M.; Hua, C. Chiral Coordination Polymers of Mandelate and its Derivatives: Tuning Crystal Packing by Modulation of Hydrogen Bonding. *Aust. J. Chem.* **2021**, *75* (2), 94–101.

[22]. Zhou, F.; Shemchuk, O.; Charpentier, M. D.; Matheys, C.; Collard, L.; ter Horst, J. H.; Leyssens, T. Simultaneous Chiral Resolution of Two Racemic Compounds by Preferential Cocrystallization. *Angew Chem Int Ed* **2021**, *60* (37), 20264–20268.

[23]. Wang, J.; Peng, Y. Resolution of Halogenated Mandelic Acids through Enantiospecific Co-Crystallization with Levetiracetam. *Molecules* **2021**, *26* (18), 5536.

[24]. Zhou, F.; Body, C.; Robeyns, K.; Leyssens, T.; Shemchuk, O. On the pairwise cocrystallization of racemic compounds. *CrystEngComm* **2023**, *25* (20), 3060–3065.

[25]. Zahoor, M.; Shafiq, S.; Ullah, H.; Sadiq, A.; Ullah, F. Isolation of quercetin and mandelic acid from Aesculus indica fruit and their biological activities. *BMC. Biochem* **2018**, *19* (1), https://doi.org/10.1186/s12858–018–0095–7.

[26]. Guo, Q.; Li, Y.; Shi, H.; Yi, A.; Xu, X.; Wang, H.; Deng, X.; Wu, Z.; Cui, Z. Novel mandelic acid derivatives suppress virulence of Ralstonia solanacearum *via* type III secretion system. *Pest Manag. Sci.* **2023**, *79* (11), 4626–4634.

[27]. Sun, Z.; Ning, Y.; Liu, L.; Liu, Y.; Sun, B.; Jiang, W.; Yang, C.; Yang, S. Metabolic engineering of the L-phenylalanine pathway in Escherichia coli for the production of S- or R-mandelic acid. *Microb Cell Fact* **2011**, *10* (1), 71 https://doi.org/10.1186/1475–2859–10–71.

[28]. Zhang, Y.; Wang, X.; Shi, H.; Siddique, F.; Xian, J.; Song, A.; Wang, B.; Wu, Z.; Cui, Z. Design and Synthesis of Mandelic Acid Derivatives for Suppression of Virulence *via* T3SS against Citrus Canker. *J. Agric. Food Chem.* **2024**, *72* (17), 9611–9620.

[29]. Sklyarenko, A. V.; Groshkova, I. A.; Gorbunov, N. A.; Vasiliev, A. V.; Kamaev, A. V.; Yarotsky, S. V. Comparative Evaluation of the Effectiveness of Biocatalytic Synthesis and Antibacterial Activity of Known Antibiotics and "Chimeric" Cephalosporin Compounds. *Appl Biochem Microbiol* **2024**, *60* (3), 431–438.

[30]. Bhavsar, S.; Tadiparthi, R.; Gupta, S.; Pawar, S.; Yeole, R.; Kayastha, A. K.; Deshpande, P.; Bhagwat, S.; Patel, M. Design and development of efficient synthetic strategies for the chiral synthesis of novel ketolide antibiotic, nafithromycin (WCK 4873). *Chem. Pap.* **2023**, *77*, 3629–3640.

[31]. Chen, J.; Lv, Q.; Tu, G. Synthesis and Molecular Simulation Studies of Mandelic Acid Peptidomimetic Derivatives as Aminopeptidase N Inhibitors. *Curr. Comput. Aided Drug Des.* **2021**, *17* (5), 619–626.

[32]. Aslani, S.; Armstrong, D. W. Fast, sensitive LC–MS resolution of alpha-hydroxy acid biomarkers via SPP-teicoplanin and an alternative UV detection approach. *Anal Bioanal Chem* **2024**, *416* (12), 3007–3017.

[33]. Widgerow, A. D.; Ziegler, M.; Garruto, J. A.; Ionescu, L.; Shafiq, F.; Meckfessel, M.; Lain, E. (.; Ablon, G.; Harper, J.; Chang, A. L.; Howard-Verovic, C. Novel Strategy for Strengthening Dermatoporotic Skin by Managing Cellular Senescence. *J. Drugs Dermatol.* **2024**, *23* (9), 748–756.

[34]. Duan, Q.; Ye, Z.; Zhou, K.; Wang, F.; Lian, C.; Shang, Y.; Liu, H. An Investigation into the Transdermal Behavior of Active Ingredients by Combination of Experiments and Multiscale Simulations. *J. Phys. Chem. B.* **2024**, *128* (26), 6327–6337.

[35]. Kopple, J. D. Phenylalanine and Tyrosine Metabolism in Chronic Kidney Failure. *J. Nutr.* **2007**, *137* (6), 1586S–1590S.

[36]. Bocato, M. Z.; Fernandes Quero, R.; Alexandre Weil, A.; Aparecida Cesila, C.; Adewuyi Adeyemi, J.; Barbosa Jr, F. A new adsorptive 3D–printed sampling device for simultaneous determination of 63 urinary organic acids by LC–MS/MS. *Anal. Chim. Acta* **2024**, *1288*, 342185.

[37]. Yevglevskis, M.; Bowskill, C. R.; Chan, C. C.; Heng, J. H.; Threadgill, M. D.; Woodman, T. J.; Lloyd, M. D. A study on the chiral inversion of mandelic acid in humans. *Org, Biomol, Chem,* **2014**, *12* (34), 6737–6744.

[38]. Poláková, M.; Krajčovičová, Z.; Meluš, V.; Štefkovičová, M.; Šulcová, M. Study of Urinary Concentrations of Mandelic Acid in Employees Exposed to Styrene. *Cent Eur J. Public Health* **2012**, *20* (3), 226–232.

[39]. Ross McDougall, I. Thyroid cancer in clinical practice; 2007th ed.; Springer: London, England, 2007.

[40]. Ivanova, B. Structural Analysis of Polylactic Acid in Composite Starch Biopolymers – A Stochastic Dynamics Mass Spectrometric Approach. *Innov Discov* **2024**, *1* (3), 26.

[41]. Ivanova, B. Stochastic dynamics mass spectrometric and Fourier transform infrared spectroscopic structural analyses of composite biodegradable plastics. *Pollut. Stud.* **2024**, *5* (2), 2741.

[42]. Cheng, Y.; Jiao, Z.; Li, M.; Xia, M.; Zhou, Z.; Song, P.; Xu, Q.; Wei, Z. A new class of nucleating agents for poly(L-lactic acid): Environmentally-friendly metal salts with biomass-derived ligands and advanced nucleation ability. *Int. J. Biol. Macromol.* **2023**, *225*, 1599–1606.

[43]. Liao, H.; Feng, B.; Song, X.; Zhang, J.; Zhang, Z. Unlocking full potential of bamboo waster: Efficient co-production of xylooligosaccharides, lignin, and glucose through low-dosage mandelic acid hydrolysis with alkaline processing. *Int. J. Biol. Macromol.* **2024**, *282*, 137165.

[44]. Wang, S.; Liu, B.; Liang, J.; Wang, F.; Bao, Y.; Qin, C.; Liang, C.; Huang, C.; Yao, S. Rapid and mild fractionation of hemicellulose through recyclable mandelic acid pretreatment. *Bioresour. Technol.* **2023**, *382*, 129154.

[45]. Jeswani, H. K.; Perry, M. R.; Shaver, M. P.; Azapagic, A. Biodegradable and conventional plastic packaging: Comparison of life cycle environmental impacts of poly(mandelic acid) and polystyrene. *Sci. Total Environ.* **2023**, *903*, 166311.

[46]. Wang, R.; Zhang, J.; Yin, Q.; Xu, Y.; Cheng, J.; Tong, R. Controlled Ring-Opening Polymerization of *O*-Carboxyanhydrides Using a β-Diiminate Zinc Catalyst. *Angew Chem Int Ed* **2016**, *55* (42), 13010–13014.

[47]. Liu, T.; Simmons, T. L.; Bohnsack, D. A.; Mackay, M. E.; Smith, M. R.; Baker, G. L. Synthesis of Polymandelide: A Degradable Polylactide Derivative with Polystyrene-like Properties. *Macromolecules* **2007**, *40* (17), 6040–6047.

[48]. Buchard, A.; Carbery, D. R.; Davidson, M. G.; Ivanova, P. K.; Jeffery, B. J.; Kociok-Köhn, G. I.; Lowe, J. P. Preparation of Stereoregular Isotactic Poly(mandelic acid) through Organocatalytic Ring-Opening Polymerization of a Cyclic *O*-Carboxyanhydride. *Angew Chem Int Ed* **2014**, *53* (50), 13858–13861.

[49]. Halder, P.; Chakraborty, B.; Banerjee, P. R.; Zangrando, E.; Paine, T. K. Role of α-hydroxycarboxylic acids in the construction of supramolecular assemblies of nickel(ii) complexes with nitrogen donor coligands. *CrystEngComm* **2009**, *11* (12), 2650.

[50]. Álvarez-Vidaurre, R.; Castiñeiras, A.; Frontera, A.; García-Santos, I.; Gil, D. M.; González-Pérez, J. M.; Niclós-Gutiérrez, J.; Torres-Iglesias, R. Weak Interactions in Cocrystals of Isoniazid with Glycolic and Mandelic Acids. *Crystals* **2021**, *11* (4), 328.

[51]. Mao, Z.; Xia, K.; Zhang, K.; Chen, H.; Li, M.; Abdukader, A.; Jin, W. Visible light-induced oxidative esterification of mandelic acid with alcohols: a new synthesis of α-ketoesters. *Green Chem.* **2024**, *26* (10), 6046–6050.

[52]. Ahsan, M. R.; Varma, H.; Mishra, M. K.; Mukherjee, A. Template-Assisted Visible Light-Induced [2 + 2] Photodimerization in a Pseudopolymorphic Binary Solid: Topotactic Transformation vs Photoinduced Crystal Melting. *Cryst. Growth amp; Des.* **2024**, *24* (12), 5193–5199.

[53]. University College London. WO2020043866 – COMPOUNDS. WO 2020/043866 A1, 2020.

[54]. van Haren, M. J.; Thomas, M. G.; Sartini, D.; Barlow, D. J.; Ramsden, D. B.; Emanuelli, M.; Klamt, F.; Martin, N. I.; Parsons, R. B. The kinetic analysis of the N-methylation of 4-phenylpyridine by nicotinamide N-methyltransferase: Evidence for a novel mechanism of substrate inhibition. *Int. J. Biochem. Cell Biol.* **2018**, *98*, 127–136.

[55]. Maris, M.; Ferri, D.; Konigsmann, L.; Mallat, T.; Baiker, A. Why are α-hydroxycarboxylic acids poor chiral modifiers for Pt in the hydrogenation of ketones?. *J. Catal.* **2006**, *237* (2), 230–236.

[56]. Fu, Y.; Liu, X.; Zhao, S. Mandelic Acid as an Interfacial Modifier for High Performance NiO_x-based Inverted Perovskite Solar Cells.

ChemNanoMat **2022**, *8* (7), e202200091 https://doi.org/10.1002/cnma.202200091.
[57]. Blessing, R. H. An empirical correction for absorption anisotropy. *Acta Crystallogr A. Found Crystallogr* **1995**, *51* (1), 33–38.
[58]. Sheldrick, G. M. A short history of *SHELX*. *Acta Crystallogr A. Found Crystallogr* **2007**, *64* (1), 112–122.
[59]. Sheldrick, G. M. Experimental phasing with *SHELXC/D/E*: combining chain tracing with density modification. *Acta Crystallogr D. Biol Crystallogr* **2010**, *66* (4), 479–485.
[60]. Sheldrick, G. M. Phase annealing in SHELX-90: direct methods for larger structures. *Acta Crystallogr A. Found Crystallogr* **1990**, *46* (6), 467–473.
[61]. Spek, A. L. Single-crystal structure validation with the program*PLATON*. *J. Appl Crystallogr* **2003**, *36* (1), 7–13.
[62]. Momma, K.; Izumi, F. *VESTA/3* for three-dimensional visualization of crystal, volumetric and morphology data. *J. Appl Crystallogr* **2011**, *44* (6), 1272–1276.
[63]. Momma, K.; Ikeda, T.; Belik, A. A.; Izumi, F. Dysnomia, a computer program for maximum-entropy method (MEM) analysis and its performance in the MEM-based pattern fitting. *Powder Diffr.* **2013**, *28* (3), 184–193.
[64]. Le Page, Y. Computer derivation of the symmetry elements implied in a structure description. *J. Appl Crystallogr* **1987**, *20* (3), 264–269.
[65]. Le Page, Y. *MISSYM*1.1 – a flexible new release. *J. Appl Crystallogr* **1988**, *21* (6), 983–984.
[66]. Spek, A. L. *CheckCIF* validation ALERTS: what they mean and how to respond. *Acta Crystallogr E. Cryst Commun* **2020**, *76* (1), 1–11.
[67]. Linden, A. Obtaining the best results: aspects of data collection, model finalization and interpretation of results in small-molecule crystal-structure determination. *Acta Crystallogr E. Cryst Commun* **2020**, *76* (6), 765–775.
[68]. Guillot, B.; Viry, L.; Guillot, R.; Lecomte, C.; Jelsch, C. Refinement of proteins at subatomic resolution with*MOPRO*. *J. Appl Crystallogr* **2001**, *34* (2), 214–223.
[69]. Farrugia, L. J. WinGX and ORTEP for Windows: an update. *J. Appl. Crystallogr*. **2012**, *45*, 849–854.
[70]. Dunitz, J. D.; Schomaker, V.; Trueblood, K. N. Interpretation of atomic displacement parameters from diffraction studies of crystals. *J. Phys. Chem.* **1988**, *92* (4), 856–867.
[71]. Dunitz, J. D.; Maverick, E. F.; Trueblood, K. N. Atomic Motions in Molecular Crystals from Diffraction Measurements. *Angew. Chem. Int. Ed. Engl.* **1988**, *27* (7), 880–895.
[72]. Hübschle, C. B.; Sheldrick, G. M.; Dittrich, B. *ShelXle*: a Qt graphical user interface for*SHELXL*. *J. Appl Crystallogr* **2011**, *44* (6), 1281–1284.
[73]. Ivanova, B. Crystallographic datasets on crystal structures measured, determined, and resolved in multiplication, *Zenodo. CERN repository* 2023. https://doi.org/10.5281/zenodo.7829163
[74]. Frisch, M. J.; Trucks, G. W.; Schlegel, H. B.; Scuseria, G. E.; Robb, M. A.; Cheeseman, J. R.; Montgomery, J. A.; Vreven, T.; Kudin, K. N.; Burant, J. C.; Millam, J. M.; Iyengar, S. S.; Tomasi, J.; Barone, V.; Mennucci, B.; Cossi, M.; Scalmani, G.; Rega, N.; Petersson, G. A.; Nakatsuji, H.; Hada, M.; Ehara, M.; Toyota, K.; Fukuda, R.; Hasegawa, J.; Ishida, M.; Nakajima, T.; Honda, Y.; Kitao, O.; Nakai, H.; Klene, M.; Li, X.; Knox, J. E.; Hratchian, H. P.; Cross, J. B.; Adamo, C.; Jaramillo, J.; Gomperts, R.; Stratmann, R. E.; Yazyev, O.; Austin, A. J.; Cammi, R.; Pomelli, C.; Ochterski, J. W.; Ayala, P. Y.; Morokuma, K.; Voth, G. A.; Salvador, P.; Dannenberg, J. J.; Zakrzewski, V. G.; Dapprich, S.; Daniels, A. D.; Strain, M. C.; Farkas, O.; Malick, D. K.; Rabuck, A. D.; Raghavachari, K; Foresman, J. B.; Ortiz, J. V.; Cui, Q.; Baboul, A. G.; Clifford, S.; Cioslowski, J.; Stefanov, B. B.; Liu, G.; Liashenko, A.; Piskorz, P.; Komaromi, I.; Martin, R. L.; Fox, D. J.; Keith, T.; Al-Laham, M. A.; Peng, C. Y.; Nanayakkara, A.; Challacombe, M.; Gill, P. M. W.; Johnson, B.; Chen, W.; Wong, M. W.; Gonzalez, C.; Pople, J. A. Gaussian 09, 98, Gaussian, Inc., Wallingford CT, 2004.
[75]. Aidas, K.; Angeli, C.; Bak, K. L.; Bakken, V.; Bast, R.; Boman, L.; Christiansen, O.; Cimiraglia, R.; Coriani, S.; Dahle, P.; Dalskov, E. K.; Ekström, U.; Enevoldsen, T.; Eriksen, J. J.; Ettenhuber, P.; Fernández, B.; Ferrighi, L.; Fliegl, H.; Frediani, L.; Hald, K.; Halkier, A.; Hättig, C.; Heiberg, H.; Helgaker, T.; Hennum, A. C.; Hettema, H.; Hjertenæs, E.; Høst, S.; Høyvik, I.-M.; Iozzi, M. F.; Jansík, B.; Jensen, H. J. A.; Jonsson, D.; Jørgensen, P.; Kauczor, J.; Kirpekar, S.; Kjærgaard, T.; Klopper, W.; Knecht, S.; Kobayashi, R.; Koch, H.; Kongsted, J.; Krapp, A.; Kristensen, K.; Ligabue, A.; Lutnæs, O. B.; Melo, J. I.; Mikkelsen, K. V.; Myhre, R. H.; Neiss, C.; Nielsen, C. B.; Norman, P.; Olsen, J.; Olsen, J. M. H.; Osted, A.; Packer, M. J.; Pawlowski, F.; Pedersen, T. B.; Provasi, P. F.; Reine, S.; Rinkevicius, Z.; Ruden, T. A.; Ruud, K.; Rybkin, V. V.; Sałek, P.; Samson, C. C. M.; de Merás, A. S.; Saue, T.; Sauer, S. P. A.; Schimmelpfennig, B.; Sneskov, K.; Steindal, A. H.; Sylvester-Hvid, K. O.; Taylor, P. R.; Teale, A. M.; Tellgren, E. I.; Tew, D. P.; Thorvaldsen, A. J.; Thøgersen, L.; Vahtras, O.; Watson, M. A.; Wilson, D. J. D.; Ziolkowski, M.; Agren, H. The Dalton quantum chemistry program system: The Dalton program. Wiley Interdiscip. Rev. Comput. Mol. Sci. 2014, 4, 269–284.
[76]. Theory and applications of computational chemistry: The first forty years; Dykstra, C. E.; Frenking, G.; Kim, K.; Scuseria, G., Eds.; Elsevier Science: London, England, 2005.
[77]. Dennington, R.; Keith, T. A.; Millam, J. M. GaussView, Version 5, Semichem Inc.; Shawnee Mission, KS, 2009.
[78]. Hartmann, M. Molecular mechanics. Von Ulrich Burkert und Norman L. Allinger. ACS Monograph 177. Washington: American Chemical Society 1982. 430 S., US $ 77.95. *Acta Polym.* **1984**, *35*, 528–528.
[79]. Allinger, N. L. Conformational analysis. 130. MM2. A hydrocarbon force field utilizing V1 and V2 torsional terms. *J. Am. Chem. Soc.* **1977**, *99* (25), 8127–8134.
[80]. Macetti, G.; Genoni, A. Quantum Mechanics/Extremely Localized Molecular Orbital Embedding Strategy for Excited States: Coupling to Time-Dependent Density Functional Theory and Equation-of-Motion Coupled Cluster. *J. Chem. Theory Comput.* **2020**, *16* (12), 7490–7506.
[81]. Stanton, J. F.; Bartlett, R. J. The equation of motion coupled-cluster method. A systematic biorthogonal approach to molecular excitation energies, transition probabilities, and excited state properties. *J. Chem. Phys.* **1993**, *98* (9), 7029–7039.
[82]. Krylov, A. I. Equation-of-Motion Coupled-Cluster Methods for Open-Shell and Electronically Excited Species: The Hitchhiker's Guide to Fock Space. *Annu. Rev. Phys. Chem.* **2008**, *59* (1), 433–462.
[83]. Reshetova, E. N. Effect of the ionic strength of a mobile phase on the chromatographic retention and thermodynamic characteristics of the adsorption of enantiomers of α-phenylcarboxylic acids on a chiral adsorbent with grafted antibiotic eremomycin. *Russ. J. Phys. Chem.* **2017**, *91* (1), 167–174.
[84]. OpenOffice. http://de.openoffice.org (accessed Feb 1, 2026).
[85]. Ivanova, B. B.; Spiteller, M. Matrixes in UV-MALDI mass spectrometry – crystals of organic salts versus co-crystals of neutral polyfunctional carboxylic acids. *Anal, Methods* **2012**, *4* (8), 2247–2253.
[86]. Marciniak, J.; Andrzejewski, M.; Cai, W.; Katrusiak, A. Wallach's Rule Enforced by Pressure in Mandelic Acid. *J. Phys. Chem. C.* **2014**, *118* (8), 4309–4313.
[87]. Cai, W.; Marciniak, J.; Andrzejewski, M.; Katrusiak, A. Pressure Effect on d,l-Mandelic Acid Racemate Crystallization. *J. Phys. Chem. C.* **2013**, *117* (14), 7279–7285.
[88]. Rose, H. A. Crystallographic Data. 61. dl-Mandelic Acid. *Anal. Chem.* **1952**, *24* (10), 1680–1681.
[89]. Wei, K. T.; Ward, D. L. α-Hydroxyphenylacetic acid: a redetermination. *Acta Crystallogr B. Struct Crystallogr Cryst Chem* **1977**, *33* (3), 797–800.
[90]. Mughal, R. K.; Gillon, A. L.; Davey, R. J. CCDC 602882: Experimental crystal structure determination 2006. http://dx.doi.org/10.5517/ccn7bt0
[91]. Fischer, A.; Profir, V. M. A metastable modification of (*RS*)-mandelic acid. *Acta Crystallogr E. Struct Rep Online* **2003**, *59* (8), o1113–o1116.
[92]. Rietveld, I. B.; Barrio, M.; Tamarit, J.; Do, B.; Céolin, R. Enantiomer Resolution by Pressure Increase: Inferences from Experimental and Topological Results for the Binary Enantiomer System (*R*)- and (*S*)-Mandelic Acid. *J. Phys. Chem. B.* **2011**, *115* (49), 14698–14703.
[93]. Ellison, R. D.; Johnson, C. K.; Levy, H. A. Glycolic acid: direct neutron diffraction determination of crystal structure and thermal motion analysis. *Acta Crystallogr B. Struct Crystallogr Cryst Chem* **1971**, *27* (2), 333–344.
[94]. Bond, A.D.; Boese, R.; Desiraju, G.R. What is a polymorph? Aspirin as a case study. *Am. Pharm. Rev.* **2007**, 10, 24–30.
[95]. Dan, Y.; Arnon, Z. A.; Tang, Y.; Kravikass, M.; Zhou, Y.; Misra, R.; Tiwari, O. S.; Shimon, L. J.; Beck, R.; Gazit, E.; Wei, G.; Adler-Abramovich, L. Effect of solvent-induced packing transitions on N-capped diphenylalanine peptide crystal growth. *Nat Commun* **2025**, *16* (1), https://doi.org/10.1038/s41467-025-61331-x.
[96]. Seidel, R.; Handrich, K.; Albéric, M.; Perrin, J.; Joester, D.; Politi, Y.; Bertinetti, L. Comparative structural analysis of stereom polymorphs in the sea urchin test. *Faraday Discuss.* **2025**, *261*, 340–358.
[97]. Guo, S.; Zhu, W.; Zhang, C. Intralayer Molecular Packing Coefficient as One Packing Characteristic of Planar Layer-Stacked Crystals and Its Dominators. *Cryst. Growth amp; Des.* **2024**, *24* (23), 9849–9856.
[98]. Vasconcelos, S. A.; Tenorio, J. C.; Gurgel, J. V.; Benevides, C. C.; Nazario, C. E.; Carvalho Jr, P. S. Polymorphism of racemic (±)-Mefloquine free base: The role of enantiomeric recognition in polymorph assemblies. *J. Mol. Struct.* **2025**, *1325*, 141043.
[99]. Rietveld, I. B.; Barrio, M.; Tamarit, J.-L.; Do, B.; Céolin, R. Enantiomer resolution by pressure increase: inferences from experimental and topological results for the binary enantiomer system (R)- and (S)-mandelic acid. *J. Phys. Chem. B* **2011**, *115*, 14698–14703.
[100]. Hylton, R. K.; Tizzard, G. J.; Threlfall, T. L.; Ellis, A. L.; Coles, S. J.; Seaton, C. C.; Schulze, E.; Lorenz, H.; Seidel-Morgenstern, A.; Stein, M.; Price, S. L. Are the Crystal Structures of Enantiopure and

Racemic Mandelic Acids Determined by Kinetics or Thermodynamics?. *J. Am. Chem. Soc.* **2015**, *137* (34), 11095–11104.
[101]. Ivanova, B. Special Issue with Research Topics on "Recent Analysis and Applications of Mass Spectra on Biochemistry". *IJMS.* **2024**, *25* (4), 1995.
[102]. Nervall, M.; Hanspers, P.; Carlsson, J.; Boukharta, L.; Åqvist, J. Predicting Binding Modes from Free Energy Calculations. *J. Med. Chem.* **2008**, *51* (9), 2657–2667.
[103]. Yung-Chi, C.; Prusoff, W. H. Relationship between the inhibition constant (KI) and the concentration of inhibitor which causes 50 per cent inhibition (I50) of an enzymatic reaction. *Biochem. Pharmacol.* **1973**, *22* (23), 3099–3108.
[104]. Wang, Y.; Su, Z.; Hsieh, C.; Chen, C. Predictions of Binding for Dopamine D2 Receptor Antagonists by the SIE Method. *J. Chem. Inf. Model.* **2009**, *49* (10), 2369–2375.
[105]. Stewart, R.; Craven, B. Molecular electrostatic potentials from crystal diffraction: the neurotransmitter gamma-aminobutyric acid. *Biophys. J.* **1993**, *65* (3), 998–1005.
[106]. Hirshfeld, F. L. Difference densities by least-squares refinement: fumaramic acid. *Acta Crystallogr B. Struct Sci* **1971**, *27* (4), 769–781.
[107]. Stewart, R. F. On the mapping of electrostatic properties from bragg diffraction data. *Chem. Phys. Lett.* **1979**, *65* (2), 335–342.
[108]. Stewart, R. Mapping electrostatic potentials from diffraction data. *God. Jugosl. Cent. Kristalogr.* **1982**, *17*, 1–24.
[109]. Spackman, M. A.; McKinnon, J. J.; Jayatilaka, D. Electrostatic potentials mapped on Hirshfeld surfaces provide direct insight into intermolecular interactions in crystals. *CrystEngComm* **2008**, *10*, 377–388.
[110]. Spackman, M. A.; Jayatilaka, D. Hirshfeld surface analysis. *CrystEngComm* **2009**, *11* (1), 19–32.
[111]. Bader, R. F. W. Atoms in Molecules: A Quantum Theory; Clarendon Press: Oxford, England, 1994.
[112]. Suda, S.; Tateno, A.; Nakane, D.; Akitsu, T. Hirshfeld Surface Analysis for Investigation of Intermolecular Interaction of Molecular Crystals. *IJOC.* **2023**, *13* (02), 57–85.
[113]. Datt, I. D.; Ozerov, R. P. Frecision study of the electronic density distributed in molecules and crystals from diffraction data. *J. Struct. Chem.* **1975**, *16*, 481–506.
[114]. Van Damme, S.; Bultinck, P.; Fias, S. Electrostatic Potentials from Self-Consistent Hirshfeld Atomic Charges. *J. Chem. Theory Comput.* **2009**, *5* (2), 334–340.
[115]. Thakur, S.; Gil, D. M.; Frontera, A.; Chattopadhyay, S. Exploration of Br···O halogen bonding interactions in dinuclear vanadium(V) complexes with Schiff base ligands. *Polyhedron* **2020**, *187*, 114676.
[116]. Hirshfeld, F. L. Bonded-atom fragments for describing molecular charge densities. *Theoret. Chim. Acta* **1977**, *44* (2), 129–138.
[117]. Hirshfeld, F. L.; Shmueli, U. Covariances of thermal parameters and their effect on rigid-body calculations. *Acta Cryst A.* **1972**, *28* (6), 648–652.
[118]. Kuriyan, J.; Petsko, G. A.; Levy, R. M.; Karplus, M. Effect of anisotropy and anharmonicity on protein crystallographic refinement. *J. Mol. Biol.* **1986**, *190* (2), 227–254.
[119]. Cruickshank, D. W. The variation of vibration amplitudes with temperature in some molecular crystals. *Acta Cryst* **1956**, *9* (12), 1005–1009.
[120]. Ivanova, B.; Spiteller, M. AgI and ZnII complexes with possible application as NLO materials – Crystal structures and properties. *Polyhedron* **2011**, *30* (2), 241–245.
[121]. Coppens, P.; Csonka, L.; Willoughby, T. V. Electron Population Parameters from Least-Squares Refinement of X-ray Diffraction Data. *Science* **1970**, *167* (3921), 1126–1128.
[122]. Mangaiyarkkarasi, J.; Saravanan, R.; Ismail, M. M. Chemical bonding and charge density distribution analysis of undoped and lanthanum doped barium titanate ceramics. *J. Chem Sci* **2016**, *128* (12), 1913–1921.
[123]. Aubert, E.; Lebègue, S.; Marsman, M.; Bui, T. T.; Jelsch, C.; Dahaoui, S.; Espinosa, E.; Ángyán, J. G. Periodic Projector Augmented Wave Density Functional Calculations on the Hexachlorobenzene Crystal and Comparison with the Experimental Multipolar Charge Density Model. *J. Phys. Chem. A.* **2011**, *115* (50), 14484–14494.
[124]. Hirano, Y.; Takeda, K.; Miki, K. Charge-density analysis of an iron–sulfur protein at an ultra-high resolution of 0.48 Å. *Nature* **2016**, *534* (7606), 281–284.
[125]. Thomas, S. P.; Pavan, M. S.; Guru Row, T. N. Experimental evidence for 'carbon bonding' in the solid state from charge density analysis. *Chem, Commun,* **2014**, *50* (1), 49–51.
[126]. Weinhold, F. Discovering chemistry with natural bond orbitals: Weinhold/discovering chemistry; John Wiley & Sons: Nashville, TN, 2012.
[127]. Brown, I. D. The chemical bond in inorganic chemistry: The bond valence model; Oxford University Press, 2006.
[128]. Brown, I. D. Recent Developments in the Methods and Applications of the Bond Valence Model. *Chem. Rev.* **2009**, *109* (12), 6858–6919.
[129]. Müller, P.; Köpke, S.; Sheldrick, G. M. Is the bond-valence method able to identify metal atoms in protein structures? *Acta Crystallogr. D Biol. Crystallogr.* **2003**, *59*, 32–37.
[130]. Escudero-Adán, E. C.; Bauzá, A.; Frontera, A.; Ballester, P. Nature of Noncovalent Carbon-Bonding Interactions Derived from Experimental Charge-Density Analysis. *ChemPhysChem* **2015**, *16* (12), 2530–2533.
[131]. Blanksby, S. J.; Ellison, G. B. Bond Dissociation Energies of Organic Molecules. *Acc. Chem. Res.* **2003**, *36* (4), 255–263.
[132]. Electron density and chemical bonding I: Experimental charge density studies; Stalke, D., Ed.; 2012th ed.; Springer: Berlin, Germany, 2014.
[133]. Ivanova, B.; Spiteller, M. On the nature of the coordination bonding of metal–organics for ions with the d 10 electronic configuration – Experimental and theoretical analyses. *Polyhedron* **2017**, *137*, 256–264.
[134]. Abramov, Y. A. On the Possibility of Kinetic Energy Density Evaluation from the Experimental Electron-Density Distribution. *Acta Crystallogr A. Found Crystallogr* **1997**, *53* (3), 264–272.
[135]. Ivanova, B.; Spiteller, M. Crystallographic and theoretical study of the atypical distorted octahedral geometry of the metal chromophore of zinc(II) bis((1R,2R)-1,2-diaminocyclohexane) dinitrate. *J. Mol. Struct.* **2022**, *1248*, 131488.
[136]. Marenich, A. V.; Jerome, S. V.; Cramer, C. J.; Truhlar, D. G. Charge Model 5: An Extension of Hirshfeld Population Analysis for the Accurate Description of Molecular Interactions in Gaseous and Condensed Phases. *J. Chem. Theory Comput.* **2012**, *8* (2), 527–541.
[137]. Badawi, H. M.; Förner, W.; Ali, S. A. A study of the solvent dependence of the structures and the vibrational, 1H and 13C NMR spectra of l- and dl-mandelic acid and l- and dl-3-phenyllactic acid. *J. Mol. Struct.* **2015**, *1093*, 150–161.
[138]. da Silva, C. C.; Guimarães, F. F.; Ribeiro, L.; Martins, F. T. Salt or cocrystal of salt? Probing the nature of multicomponent crystal forms with infrared spectroscopy. *Spectrochim. Acta A: Mol. Biomol. Spectrosc.* **2016**, *167*, 89–95.
[139]. Wang, Z.; Duan, S.; Zhang, R.; Ma, L.; Lin, K. Rapid chiral purity identification of mandelic acid by Raman spectra in the O–H stretching region. *Spectrochim. Acta A: Mol. Biomol. Spectrosc.* **2023**, *303*, 123251.
[140]. Barth, G.; Voelter, W.; Mosher, H. S.; Bunnenberg, E.; Djerassi, C. Optical rotatory dispersion studies. CXVII. Absolute configurational assignments of some .alpha.-substituted phenylacetic acids by circular dichroism measurements. *J. Am. Chem. Soc.* **1970**, *92*, 875–886.
[141]. Ivanova, B.; Spiteller, M. Stochastic dynamic electrospray ionization mass spectrometric diffusion parameters and 3D structural determination of complexes of AgI–ion – Experimental and theoretical treatment. *J. Mol. Liq.* **2019**, *292*, 111307.